ELSEVIER

Journal of Power Sources 65 (1997) 159–171

JOURNAL OF POWER SOURCES

25

Performance and modelling of a direct methanol solid polymer electrolyte fuel cell

K. Scott [a,*], W. Taama [a], J. Cruickshank [b]

[a] *Department of Chemical and Process Engineering, University of Newcastle, Newcastle upon Tyne NE1 7RU, UK*

[b] *Defence Evaluation and Research Agency, Haslar, Gosport, Hants PO12 2AG, UK*

Received 4 November 1996; accepted 30 November 1996

Abstract

The performance and modelling of a direct methanol fuel cell based on a solid polymer electrolyte membrane (SPE) is reported. Two sizes of cell are used: a small cell with an area of 9 cm^2 and a large single cell with an area of 250 cm^2. The fuel cell utilises a vapourised methanol fuel at a porous carbon/Pt–Ru catalyst electrode. The performance of the fuel cell is affected by the cross-over of methanol from the anode to the cathode through the polymer membrane and this behaviour is modelled. To evaluate cell performance, mathematical models are constructed which describe mass transport in the porous electrode structures and the potential and concentration distributions in the electrode regions. These models are used to predict the cell voltage and current density response of the fuel cell.

Keywords: Fuel cells/solid polymer electrolyte; Mathematical modelling

1. Introduction

The direct methanol fuel cell (DMFC) uses methanol, in the form of vapour or liquid, to generate electrical energy. Advancements in electrocatalysis have enabled this electrochemical combustion to carbon dioxide to proceed without the formation of intermediate products [1]:
anode:

$$CH_3OH + H_2O = CO_2 + 6H^+ + 6e^- \quad (1)$$

cathode:

$$3/2O_2 + 6H^+ + 6e^- = 3H_2O \quad (2)$$

The thermodynamic reversible cell potential for this overall reaction is 1.214 V, which is very close to that of 1.23 V for the hydrogen fuel cell, and consequently has generated the interest in the DMFC as an alternative power source. Fuel cells generally, among their many uses, are expected to fill an important role in the replacement of the internal combustion engine. The DMFC has several advantages which suit its application to transportation, including high efficiency, very low emissions, a potentially renewable fuel source and fast and convenient refuelling. This latter feature is considered to be significant in the planning of fuel supply systems which could be based on the infrastructure already in existence for internal combustion engines. Hydrogen-based fuel systems are less convenient, requiring much more sophisticated storage and transportation. Alternatively, reformation of methanol on board a vehicle is possible although a significant weight and volume penalty results.

The current advantage of the hydrogen cell is that hydrogen oxidation at the anode is very fast and consequently the performance of the hydrogen cell is better than that of the methanol cell. The major loss in voltage of hydrogen fuel cells, at low to moderate current densities, is due to oxygen reduction. This requires four electrons in comparison to the two electrons required in hydrogen oxidation. For methanol, six electrons must be exchanged for complete oxidation and consequently the oxidation kinetics are inherently slower. A factor of the slower kinetics is believed to be 'poisoning' of the anode catalyst by intermediates formed during methanol oxidation [2]. Oxidation of the poisoning intermediates to carbon dioxide requires the adsorption of an oxygen containing species (e.g. OH, H_2O). Adsorption of these species does not occur substantially until potentials well above the open-circuit values are used [3]. Platinum by itself is not sufficiently active to be a commercial methanol oxidation electrocatalyst. Consequently significant activity has been seen in the promotion of methanol oxidation with significant results achieved with the use of binary catalysts, notably Pt–Ru, where the second metal forms a surface oxide in the

* Corresponding author.

PII S0378-7753(97)02485-3

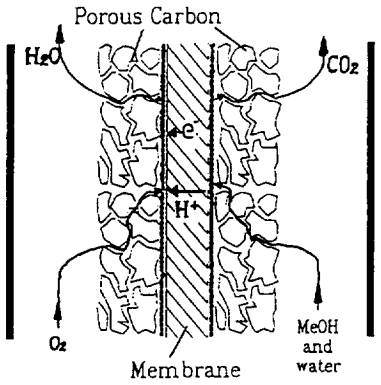

Fig. 1. A schematic diagram of the direct methanol fuel cell with solid polymer electrolyte.

potential range for methanol oxidation [4]. The area of methanol oxidation catalysis needs further performance improvements to push the DMFC towards successful commercial exploitation and research is ongoing in several laboratories worldwide.

The DMFC can function in several electrolytes; alkaline, acid and proton conducting polymer. Alkaline electrolytes pose the problem of carbonation and research efforts have focused on acid electrolyte and more recently solid polymer electrolytes (see Fig. 1). Much of the research on SPE systems has used Nafion® membranes, typically 117, from DuPont. The direct methanol fuel cell based upon solid polymer electrolyte (SPE) has the additional advantage of no liquid acidic or alkaline electrolyte. Recent developments in electrode fabrication techniques and better cell designs have brought dramatic improvements in cell performance in small-scale DMFCs. Typically, power densities higher than 0.18 W cm^{-2} are achievable, and power densities higher than 0.3 W cm^{-2} have been reported [5]. These power densities are however substantially lower than those obtained with hydrogen fuel cells, 0.6–0.7 W cm^{-2}, with which loading of the platinum anode catalyst can be substantially lower (0.1 mg Pt cm^{-2}).

To date an essential condition for the successful operation of a DMFC is the use of a pressurised oxygen or air supply to the cathode. Another important factor is the concentration of methanol in the water–methanol mixture fed to the anode. At concentrations higher than around 2 molar, the cell voltage declines significantly due to poisoning of the cathode electrocatalyst by methanol that has permeated through the SPE (Nafion®) membrane, i.e. methanol crossover. We have measured permeation rates of water and methanol using a membrane-electrode assembly (MEA) and membrane alone, installed in a small-scale cell assembly under typical DMFC operating conditions. The results obtained have been used to explain the relatively poor performance of the DMFC when low pressure oxygen and when high concentrations of methanol are used [6]. Thus a second area for research to improve the DMFC performance is in polymer membrane electrolytes. Recent work has reported the use of polybenzimidazole [7] and perfluorinated sulfonimides [8] as polymer electrolyte membranes as a means of reducing the impact of methanol crossover.

The research reported here relates to a programme geared to the scale up of the DMFC to a stack with a power output of 0.5 kW. Data presented are for single cell performance of the DMFC using Nafion® 117 membranes and the modelling of the cell to predict the cell voltage and current density characteristics.

2. Experimental

Tests on the DMFC were performed with two cells, one with a cross-sectional area of 9 cm^2 and the second with a cross-sectional area of 250 cm^2. Each cell was fitted with one membrane electrode assembly (MEA) of the appropriate size. In the small cell the MEA was sandwiched between two graphite paper gaskets (see Fig. 2), with serpentine flow paths cut out for methanol and oxygen/air flow, and then between solid graphite blocks with fluid entry ports. The cell was held together between two aluminum backing plates using a set of retaining bolts positioned around the periphery of the cell. In the larger cell the MEA was sandwiched between two graphite blocks into which the flow paths for methanol and air were cut. The flow path consisted of a set of small rectangular channels (1 mm by 1 mm) arranged in a serpentine flow path (Fig. 3). The fuel cells were used in a simple flow rig (shown schematically in Fig. 4) which consisted of a Watson Marlow perilstatic pump to supply aqueous methanol solution from a reservoir, and a Eurotherm temperature controller to heat and vaporise the methanol. Air was supplied from cylinders at ambient temperature, bubbled through water for humidification, and the pressure regulated at inlet by pressure regulating valves. All connections between the cells and equipment were with PTFE tubing, fittings and valves. The output from the cathode side of the cell was analysed on-line using an AI Cambridge GC94 gas chromatograph.

MEAs studied in this work were made in the following manner. The anode consisted of a carbon cloth support (E-Tek, type 'A') upon which was spread a thin layer of uncatalysed (ketjenblack 600) carbon, bound with 10 wt.%

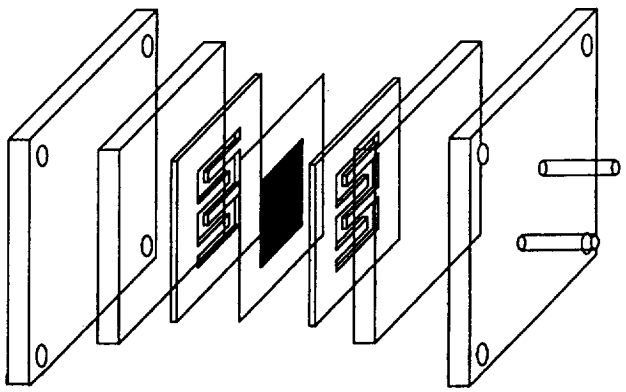

Fig. 2. Schematic diagram of the experimental small scale DMFC.

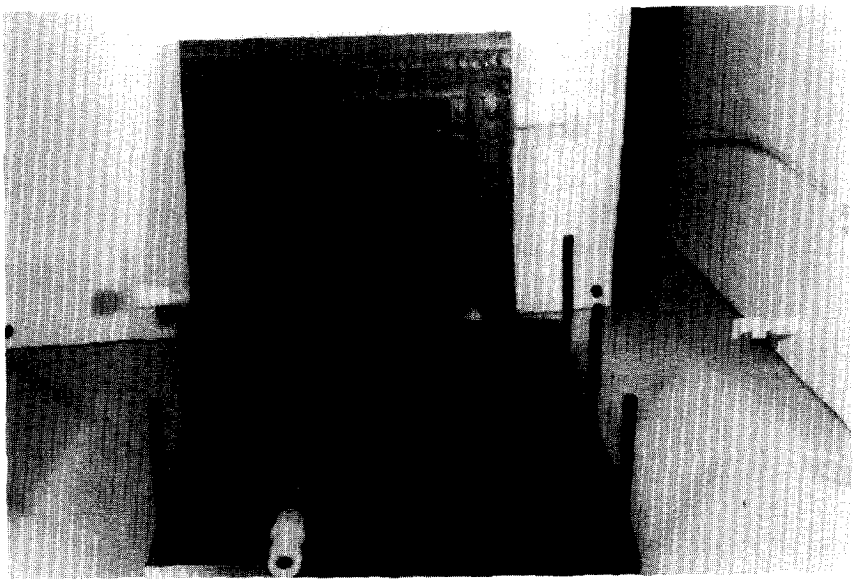

Fig. 3. Photograph of the large scale DMFC showing the serpentine flow beds.

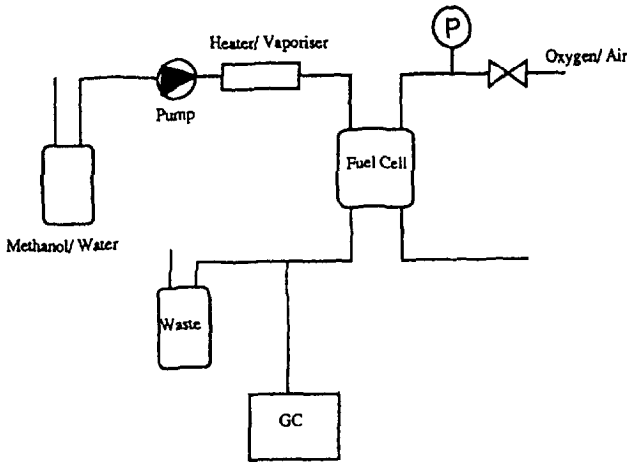

Fig. 4. Schematic diagram of the experimental DMFC flow circuit.

Nafion® from a solution of 5 wt.% Nafion® dissolved in a mixture of water and lower aliphatic alcohols (Aldrich).

The catalysed layer, consisting of 50 wt.% Pt–Ru (2 mg cm^{-2} metal loading) dispersed on carbon (ketjen) and bound with 10 wt.% Nafion®, was spread on this diffusion backing layer. The cathode was constructed similarly, using a diffusion layer bound with 15 wt.% PTFE, and 1 mg cm^{-2} Pt black (Aldrich) with 10 wt.% Nafion® as the catalyst layer. The purpose of the uncatalysed layers was primarily to provide a flat surface for the catalyst. The electrodes were placed either side of a Nafion® 117 membrane (Aldrich), which had been previously boiled for 1 h in 5 vol.% H_2O_2 and 1 h in 1 M H_2SO_4 before washing in boiling Millipore water ($< 18\ m\Omega$) for 2 h with regular changes of water. The assembly was hot-pressed at 100 kg cm^{-2} for 3 min at 135°C. The resulting MEA was installed in the cell after pressing, and hydrated with water circulated over the anode at 96°C for several hours.

3. Mathematical model of the DMFC MEA assembly

The model structure of the DMFC, shown in Fig. 5, consists of a flow channel cut into a graphite flow-bed, through which the reactant flows: adjacent to the channel is the diffusion region of the electrode, comprised of a highly-porous

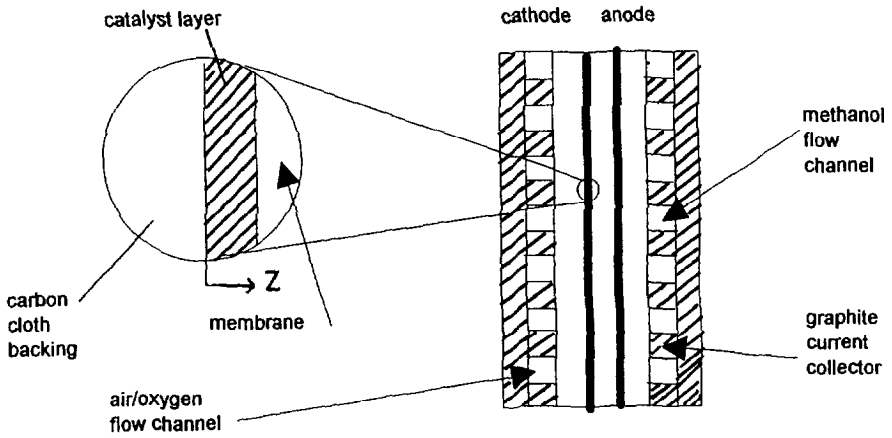

Fig. 5. Model of the DMFC structure.

carbon cloth backing layer and a thin layer of uncatalysed Nafion-bound carbon black. Next comes the layer of porous electrocatalyst, followed by the Nafion membrane. A similar structure exists on the other side of the membrane. The model for the DMFC needs to account for changes in potential and allow for the transfer of methanol from the anode to the cathode and its effect on the performance of the cathode.

The model for diffusion through the carbon fibre cloth adjacent to the electrocatalyst layers is presented in the Appendix for the case of the methanol anode side of the cell. The effect of diffusion through the highly porous structure is negligible under realistic operating conditions. Similar conclusions can also be made for the oxygen cathode side of the cell.

The major assumptions adopted in the model are as follows.

(i) Due to the high thermal conductivities of the graphite and aluminum cell components, the cell temperature is assumed to be constant and uniform.

(ii) Transport along the flow channels can be described by plug flow.

(iii) The pressure is uniform within each cell compartment — any pressure drop occurs across the membrane.

(iv) Due to the thinness of the diffusion region of the electrodes, transport in this region is not considered.

(v) Due to the high electronic conductivity of the carbon substrate and graphite flow-beds, no voltage drop is considered to occur through the thickness of the electrode, or along the flow channels.

(vi) Due to the amount of water in the anode flow channels, the membrane is considered to be fully hydrated.

(vii) The concentration of reactant is taken as the weighted average of the inlet and outlet concentrations.

(viii) Electrode kinetics can be described by the Tafel equation.

(ix) The overpotential caused by methanol crossover is directly proportional to the concentration of methanol at the cathode.

The object of the model is to calculate the overall cell voltage, which can be written as:

$$V_{cell} = E_{cell} - \eta_{an} - \eta_{cat} - \eta_{xover} - \eta_{ohmic} \quad (3)$$

where E_{cell} is the difference between the half-cell potentials of the anode and cathode, at the reference current density i_0, corrected for the thermodynamic effects of temperature and pressure. In the first instance we consider that the anode and cathode overpotentials η_{an} and η_{cat} are described by Tafel kinetics at the electrodes, and a one-dimensional potential and concentration distribution is calculated within the thickness of the catalyst layers. Ohmic overpotential, η_{ohmic}, is calculated for the resistance of the membrane, and the effect of methanol crossover, i.e. the crossover overpotential, η_{xover}, is calculated from the flux of methanol through the membrane. The appropriate expressions for these potential contributions are:

$$E_{cell} = E^0_{cell} + \Delta T\left(\frac{\partial E}{\partial T}\right) - \Delta N\frac{RT}{nF}\ln\left(\frac{P_2}{P_1}\right) \quad (4)$$

$$\eta_{ohmic} = \frac{It_m}{\sigma_m} \quad (5)$$

$$\eta_{xover} = \chi j_{MeOH} \quad (6)$$

3.1. Methanol permeation through the membrane

Permeation of water and/or methanol through a Nafion® membrane will take place under the driving forces of concentration and pressure gradients, and electro-osmosis. If we assume Fickian diffusion and a linear concentration gradient through the membrane of thickness t_m (i.e. the effective diffusivity is independent of concentration), then we can write:

$$j = -\frac{D}{t_m}\Delta c - \frac{c_2 K}{t_m}\Delta P + \frac{\lambda}{nF}I \quad (7)$$

Assuming that the permeate is entrained in the carrier gas flow at a rate proportional to c_2, we can write:

$$j = kc_2 \quad (8)$$

Combining Eqs. (7) and (8):

$$j = \left(\frac{Dc_1}{t_m} + \frac{\lambda}{F}I\right)\Big/\left(1 + \frac{D}{kt_m} + \frac{K}{kt_m}\Delta P\right) \quad (9)$$

We have measured permeation rates for water, methanol and a water–methanol mixture through Nafion® 117 and calculated the values of k and K from the data [6]. To describe the effect of methanol flux on the cathode performance we assume a methanol coverage, θ, proportional to the methanol concentration:

$$\theta \propto c_{2,\,MeOH} \quad (10)$$

Assuming that the methanol-covered fraction of the surface area has a lower free energy for oxygen reduction, in which case the overpotential produced by methanol crossover is proportional to the flux then,

$$\eta_{xover} = \chi j_{MeOH} \quad (11)$$

where χ is an empirical constant to be determined.

This model predicts, then, that the overpotential due to methanol crossover will have a current-independent term, affected by the pressure differential, and a current-dependent term (producing an iR-like drop) due to electro-osmosis of methanol. By measuring the effect of pressure differential on flux and on overpotential (correcting for kinetic effects) we can determine a value for χ and then estimate λ_{MeOH}.

From the results of the correlation of methanol permeation data and the calculation of the appropriate parameters, a simple model, based on linear electrode kinetics, has been produced based on Eq. (7) which describes the impact of methanol permeation on the cell current density–voltage response. The model data correlation and experiment are in

good agreement [6], in the current density range 50–350 mA cm^{-2}, which is the range of practical operation. At low current densities the model is not expected to agree due to the assumption of linear kinetics. With the introduction of Butler–Volmer kinetics the model gives a good fit over the current density range up to 350 mA cm^{-2}.

3.1.1. Porous electrocatalyst layer model

The model is used to predict the current distribution within the porous electrode caused by a mixture of poor mass transport (diffusion) and low protonic conductivity. Each electrode region is described by the same model structure with different parameters used in the appropriate solution. To illustrate the model, an oxygen consuming cathode is considered as shown in Fig 5. As oxygen diffuses into the electrode, it will be consumed at a rate governed by the local effective overpotential, $\eta(z)$, and the local concentration $c(z)$, where z is the distance into the electrode. Assuming a Tafel relationship, the local current density, $i(z)$, can be written as:

$$i(z) = i_o c(z)/c_o \exp\{\eta(z)/\beta\} \tag{12}$$

where, i_o is the exchange current density at the reference potential, c_o is the reactant concentration at the oxygen/electrode interface, and β is a constant related to the Tafel slope.

Fig. 5 shows a representation of the porous electrode of thickness l, with the oxygen/electrode interface at $z=0$ and the electrode/membrane interface at $z=1$. Protonic resistivity within the electrode is given by ρ, the effective catalyst surface area per unit volume is γ, and D denotes the effective reactant diffusivity within the porous electrode.

If we consider the potential drop across a small distance δz of the electrode, we can write Ohm's law as:

$$\phi(z+\delta z) - \phi(z) = \rho \delta z \int_0^z yj(z)\,dz \tag{13}$$

where $\phi(z)$ is the potential of the proton-conducting phase within the electrode. In the limit, as $\delta z \to 0$:

$$\frac{d\phi(z)}{dz} = \rho\gamma \int_0^z (z)\,dz \tag{14}$$

The measured overpotential, E, is the difference between the potential of the electronic conducting phase, ϕ_c (assumed to have negligible resistivity), and the membrane $\phi(l)$, minus the reference potential difference, $\Delta\phi_0$

$$E = \phi_c - \phi(l) - \Delta\phi_0 \tag{15}$$

The effective overpotential at any point within the electrode can be written as:

$$\eta(z) = \phi_c - \phi(z) - \Delta\phi_0 \tag{16}$$

Therefore, by differentiating Eq. (14) w.r.t. z, we obtain:

$$\frac{d^2\eta(z)}{dz^2} = \rho\gamma i(z) \tag{17}$$

Now, the rate at which the flux of reactant (gradient of concentration) is changing within the electrode is related directly to the local current density, and can be written as:

$$\frac{d^2c(z)}{dz^2} = \frac{\gamma}{DnF} i(z) \tag{18}$$

where F is Faraday's constant and n is the number of electrons involved in the reaction.

Eqs. (17) and (18) fully describe the variation in concentration and effective overpotential as a function of the distance through the electrode. The boundary values relevant to this problem are:

$$c(0) = C_0, \left.\frac{dc}{dz}\right|_1 = 0 \tag{19}$$

$$\left.\frac{d\eta}{dz}\right|_0 = 0, \ \eta(I) = E_r \tag{20}$$

The solution of these Eqs. can be simplified by adopting reduced variables as follows:

$$\bar{z} = \frac{z}{1}, \ \bar{C} = \frac{C}{C_0}, \ \bar{\eta} = \frac{\eta}{E_r}, \ \bar{\imath} = \frac{i}{i_0} \tag{21}$$

so that

$$\frac{d^2\bar{\eta}}{d\bar{z}^2} = \left(\frac{l^2}{E}\rho\gamma i_o\right)\bar{c}\exp\left\{\frac{E}{\beta}\bar{\eta}\right\} \tag{22}$$

$$\frac{d^2\bar{C}}{d\bar{z}^2} = \left(\frac{l^2}{C_0}\frac{\gamma i_0}{DnF}\right)\bar{c}\exp\left\{\frac{E}{\beta}\bar{\eta}\right\} \tag{23}$$

In the case of the methanol-consuming anode, an additional term should, in principle, be considered in the material balance equation describing the effect of methanol crossover by an electro-osmotic drag term. It is assumed that the extent of this methanol drag is defined by a drag factor n_{drag}, the moles of methanol transferred per mole of proton, and the local methanol drag is given by:

molar methanol flux,

$$N_{meth} = n_{drag} i(z)/F \tag{24}$$

The change in the local methanol drag is given by:

$$dN_{meth}/dz = n_{drag}/F\ di(z)/dz = (n_{drag}/F) i(z)\gamma \tag{25}$$

The material balance then becomes:

$$\frac{d^2c(z)}{dz^2} = \frac{\gamma}{DnF} i(z)(1 + nn_{drag}) \tag{26}$$

Thus in the general solution of the model the inclusion of a methanol electro-osmotic drag term modifies the term M_2 defined below.

Overall the basic equations which enable the calculation of the voltage components in Eq. (3) are:

$$\frac{d^2\bar{\eta}_r}{d\bar{z}_r^2} = M_{1,r}\bar{c}_r \exp(M_{3,r}\bar{\eta}_r), \ \frac{d^2\bar{c}_r}{d\bar{z}_r^2} = M_{2,r}\bar{c}_r \exp(M_{3,r}\bar{\eta}_r)$$

subscript r refers to the region considered (anode or cathode electrocatalyst layer).

$$\bar{z}=\frac{z}{l},\ \bar{\eta}=\frac{\eta_{\mathrm{loc}}}{E_{\mathrm{r}}},\ \bar{c}=\frac{c_{\mathrm{loc,\,reac}}}{c_{\mathrm{o,\,reac}}}$$

$$M_1=\left(\frac{l^2\rho\gamma i_0}{E_{\mathrm{r}}}\right),\ M_2=\left(\frac{l^2\gamma i_0}{c_{\mathrm{o,\,reac}}D_{\mathrm{eff}}nF}\right),\ M_3=\frac{E_{\mathrm{r}}}{b}$$

$$j_{\mathrm{MeOH}}=-\frac{D_{\mathrm{m,MeOH}}}{t_{\mathrm{m}}}\Delta C_{\mathrm{m,MeOH}}-\frac{C_{\mathrm{cat,MeOH}}K}{t_{\mathrm{m}}}\Delta P+\frac{\gamma_{\mathrm{MeOH}}}{n_{\mathrm{an}}F}I$$

$$\rho_{\mathrm{r}}=\frac{1}{\sigma_{\mathrm{m}}}\nu_{\mathrm{m}},\ \gamma_{\mathrm{MeOH}}\cong x^0_{\mathrm{MeOH}}\lambda_{\mathrm{H_2O}}$$

3.1.2. Method of solution

The method of solution requires that the models of the catalyst layers give the required overpotentials. In this a value for η_{cat} is chosen, and I is calculated. A value for η_{an} is obtained using the given I. The values of E_{cell}, η_{ohmic} and η_{xover} are then calculated, to obtain the final cell voltage, V_{cell}.

The equations describing the concentration and potential distribution within the electrode are solved numerically using the finite-difference method and Newman's BAND algorithm for the resulting simultaneous non-linear equations (using modified NL3BAND.C software [9,10]). To obtain a prescribed value of I, iteration using a Newton-type algorithm is employed:

$$E^{k+1}=E^k-\frac{I(E^k)-E_{\mathrm{given}}}{I'(E^k)}$$

$$I'(E^k)=\frac{I(E^k+\delta)-I(E^k)}{\delta}$$

where δ was typically $\approx 10^{-4}\times E$. The subscript refers to the k^{th} iterate from a guessed value.

3.1.3. Temperature effect on cell voltage

From thermodynamics:

$$\left(\frac{\partial E}{\partial T}\right)_P=\frac{\Delta S}{nF}$$

where E is the electric potential. Assuming ΔS is constant over the temperature range considered, then the change in cell voltage can be written as:

$$\Delta T\cdot\frac{\Delta S}{nF}$$

For the methanol oxidation reaction:

$$CH_3OH+\frac{3}{2}O_2\rightarrow CO_2+2H_2O$$

we can calculate from standard thermodynamic data (at 25°C), where the methanol and water are liquid:

$\Delta H=-726.51\ \mathrm{kJ\ mol^{-1}}$, $\Delta G=-702.36\ \mathrm{kJ\ mol^{-1}}$,

$\Delta S=-0.081\ \mathrm{kJ\ mol^{-1}\ K^{-1}}$

and for the gaseous case:

$\Delta H=-709.33\ \mathrm{kJ\ mol^{-1}}$, $\Delta G=-889.42\ \mathrm{kJ\ mol^{-1}}$,

$\Delta S=+0.604\ \mathrm{kJ\ mol^{-1}\ K^{-1}}$

so that:

$$\left(\frac{\partial E}{\partial T}\right)_{\mathrm{liq}}=-0.140\ \mathrm{mV\ K^{-1}},\ \left(\frac{\partial E}{\partial T}\right)_{\mathrm{gas}}=+1.043\ \mathrm{mV\ K^{-1}}$$

3.1.4. Pressure effect on cell voltage

From thermodynamics:

$$\left(\frac{\partial E}{\partial P}\right)_T=-\frac{\Delta V}{nF}$$

which gives, on integration:

$$\Delta E=-\frac{\Delta NRT}{nF}\ln\left(\frac{P_2}{P_1}\right)$$

For the oxygen reduction reaction:

$$2H^++\frac{1}{2}O_2+2e^-\rightarrow H_2O$$

we get ΔN for the liquid and gaseous cases as -0.5 and $+0.5$, respectively. At 80°C, increasing the pressure to 2 bar will increase the voltage by 10.5 mV.

3.1.5. Conductivity of Nafion

This can be described by the following relation [11]:

$$\sigma_{\mathrm{m}}=\sigma_{\mathrm{m}}^{\mathrm{ref}}\exp\left[1268\left(\frac{1}{T_{\mathrm{ref}}}-\frac{1}{T}\right)\right]$$

As a reference point, we use a.c. measurements performed in our laboratory which give the conductivity as 0.073 ± 0.008 S cm, with a similar value for recast Nafion films, at 25°C. This gives:

$$\sigma_{\mathrm{m}}=0.073\exp\left[1268\left(\frac{1}{298}-\frac{1}{T}\right)\right]\ \mathrm{S\ cm}$$

3.1.6. Diffusion coefficients of water and methanol in Nafion 117

The variation of diffusivity with temperature can generally be described by an equation of the form:

$$D_{\mathrm{i}}=D_{\mathrm{i,\,ref}}\exp\left[\frac{\Delta E}{R}\left(\frac{1}{T_{\mathrm{ref}}}-\frac{1}{T}\right)\right]$$

For the diffusion of water through Nafion 1155 E.W., Yeo and Eisenberg [12] calculated a value for $\Delta E/R$ of 2416 K. Springer et al. [13] found a value of 2436 K.

We will use the latter value, as it pertains to measurements on Nafion 117. For a reference value, we use the PGSE measurements of Zawodzinski and Springer [14] which give:

$D_{m,\,water} = 7.3\times10^{-6}\ cm^2\ s^{-1}$ @80°C

so that:

$$D_{m,\,water} = 7.3\times10^{-6}\exp\left[2436\left(\frac{1}{353}-\frac{1}{T}\right)\right]$$

For methanol in Nafion, we use the same activation energy as for water, since there is a paucity of results in this area. For a reference point, we refer to the work of Kauranen and Skou [15] who measured a (superficial) diffusivity:

$D_{m,\,MeOH} = 4.9\times10^{-6}\ cm^2\ s^{-1}$ @60°C

giving:

$$D_{m,\,MeOH} = 4.9\times10^{-6}\exp\left[2436\left(\frac{1}{333}-\frac{1}{T}\right)\right]$$

3.1.7. Diffusion coefficients in the catalyst layers

The diffusion of methanol in the catalyst layer is assumed to have a similar temperature dependence. Using a reference value for methanol in water at 80°C given by Kauranen and Skou [15], so that:

$$D_{r,\,MeOH} = 2.8\times10^{-5}\exp\left[2436\left(\frac{1}{353}-\frac{1}{T}\right)\right]$$

When multiplied by the porosity-tortuosity factor, ϵ, we obtain the effective diffusion coefficient.The value of λ_{MeOH} is assumed to be given simply by:

$$\lambda_{MeOH} = x^0_{MeOH}\lambda_{H_2O}$$

where λ_{H_2O} has been given by Zawodzinski and Springer [14] as 2.0–2.9 H_2O/H^+ in fully hydrated Nafion 117. We will use the average value of 2.5.

3.1.8. Dependence of i_0 on temperature

Parthasarathy et al. [16] have given the temperature dependence of the electrode kinetics of oxygen reduction as

$$i_{0,\,cat} = i^{ref}_{0,\,cat}\exp\left[8804\left(\frac{1}{T_{ref}}-\frac{1}{T}\right)\right]$$

For methanol oxidation at the anode, Troughton [1] has measured the activation energy for a Pt–Ru supported catalyst as 70 kJ mol^{-1}, giving:

$$i_{0,\,an} = i^{ref}_{0,\,an}\exp\left[8420\left(\frac{1}{T_{ref}}-\frac{1}{T}\right)\right]$$

The Tafel slope for the oxidation reaction can also be estimated from Troughton's work as 46 mV/factor of e at 80°C.

3.1.9. Concentrations

A methanol concentration of one molar translates into the following value for the mole fraction:

$c_{0,\,MeOH} = 1\times10^{-3}\ mol\ cm^{-3}$

$x_{0,\,MeOH} = 0.0184$

For the oxygen concentration at the cathode, we assume ideal gas properties, so that:

$$c_{0,\,O_2} = \frac{P}{10\times RT}\ mol\ cm^{-3}$$

4. Results and discussion

One purpose of the model is to estimate the variation in local reactant concentration and potential to predict the total polarisation potential at both electrodes. Figs. 6 and 7 show the typical distribution of potential, concentrations and current density for the cathode and the anode, respectively. The activity of the electrode, seen in terms of local current density and overpotential, is higher near to the membrane and decreases towards the carbon backing layers as current tends to follow the more conductive electronic path through the electrode structure. In the case of the cathode, at what is a relatively low overall current density of approximately 62 mA cm^{-2}, there is an approximate 25% reduction in the oxygen concentration from the gas side towards the membrane. The extent of the overall polarisation of the electrode depends on several parameters and notably the thickness of the electrode. The data in Fig. 6 are for a relatively thick oxygen electrode (200 μm). The overall potential versus current density for this electrode is shown in Fig. 8. The effective Tafel slope for the electrode is approximately twice that for a non-porous electrode, i.e. the extent of polarisation of the electrode is increased as a result of the distribution of current in the porous structure. This behaviour corresponds with that predicted by simple models of the electrode based on an assumption of a constant overpotential in the electrode, derived from Eq. (8). This predicts for thick electrodes (or high current densities, poor diffusion) that the total current is given by:

$$I = nFDC_o\gamma i_o\exp(\eta/2\beta)$$

The distribution of methanol concentration and overpotential in the porous anode, as shown in Fig 7, is for a high value of overall current density at a thin catalytic electrode (5 μm). The extent of polarisation produced by the porous electrode is relatively small even though there is a large change in the methanol concentration through the electrode structure.

The complete model of the MEA is used to predict the variation of cell potential with overall current density, both with and without the influence of methanol crossover. The experimental work has shown that there is a significant effect of increasing the oxygen pressure on cell performance which cannot be predicted from thermodynamic or kinetic behaviour or by the model which does not allow for the effect of methanol crossover, as shown in Fig. 9. The predictions in Fig. 9 represent the ideal fuel cell characteristics if methanol crossover could be eliminated. When the factor of methanol crossover is introduced there is a significant change in the cell characteristics (see Fig. 10), cell voltages are signifi-

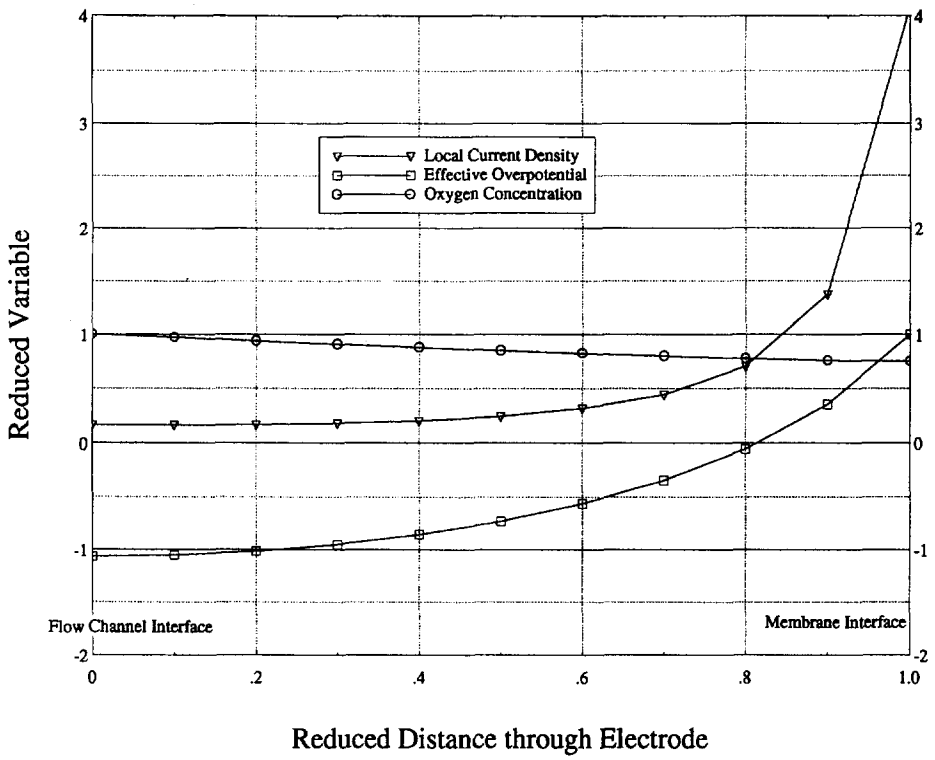

Fig. 6. Variation in the local values of concentration of oxygen, overpotential and current density in the oxygen cathode. $M_2 = 16$, $M_3 = 0.6$, $E_r = 0.1$, $\beta = 0.06$.

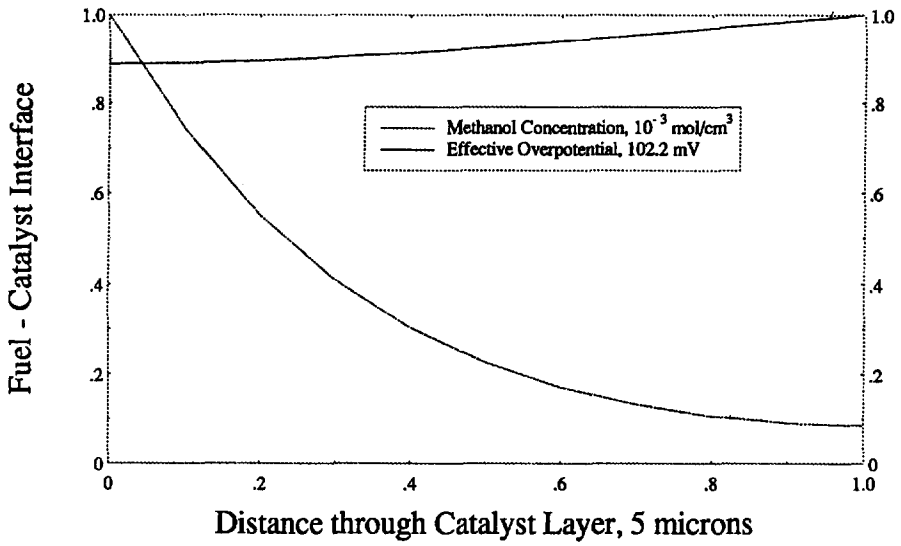

Fig. 7. Variation in the local methanol concentration and overpotential in the anode. $I = 938$ mA cm^{-2}. Methanol feed concentration = 1.0 kmol m^{-3}.

cantly lower and decrease when the oxygen pressure is reduced.

The agreement between the model and the experimental data for the small scale cell (see Fig. 10) is good over a significant range of practical operating current densities, up to approximately 350–400 mA cm^{-2}. The poorer agreement at low current densities is partly due to the assumption of Tafel kinetics and the relatively simple model for the effect of poisoning of the cathode due to methanol.

The experimental data shown in Fig. 10 are for a relatively low operating temperature of 80°C. The maximum power densities are of the order of 0.2 W cm^{-2}. Power densities reported by other researchers are generally at higher temperatures, for example Ren et al. [17] report values of 0.38 W cm^{-2} at 130°C, using oxygen at a pressure of 5 bar, and 0.25 W cm^{-2} at 110°C using air at 3 bar. A difference of 50°C in the operating temperature makes a significant difference in the cell performance. For example, at a constant cell voltage of 0.5, Ren et al. report a reduction in current density from around 450 mA cm^{-2} to about 170 mA cm^{-2} when the temperature is reduced from 130 to 80°C. In addition, these values were obtained using Nafion 112 membrane as opposed to the Nafion 117 used in this work. Nafion 112 shows approximately half the cell resistance of Nafion 117 when used in a

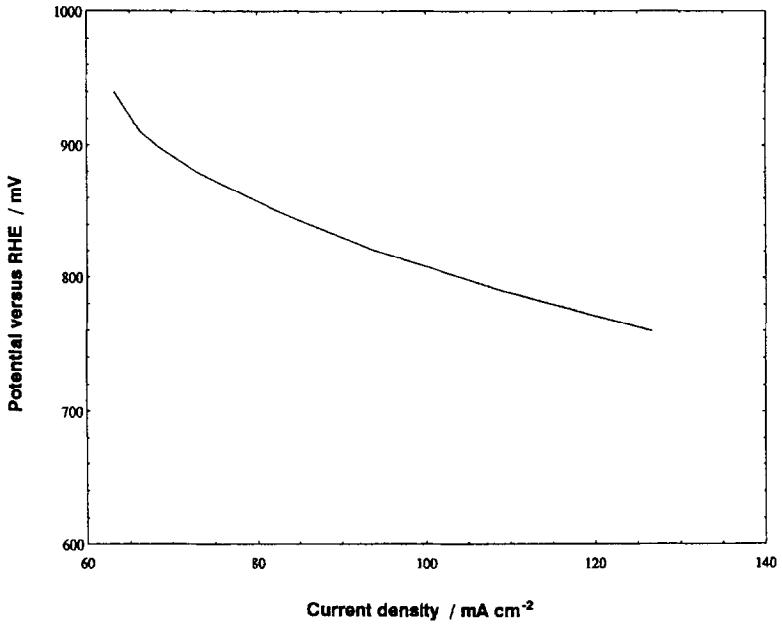

Fig. 8. Predicted variation in the cathode potential, current density characteristics for the oxygen cathode. $M_2 = 16$, $M_3 = 0.6$, $E_r = 0.1$, $i_o = 0.01$, $D = 0.1$ cm^2 s^{-1}, $c_o = 3\,e^{-5}$ mol m^{-3}.

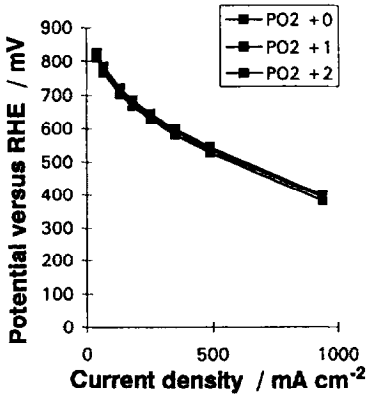

Fig. 9. Performance of the DMFC without methanol crossover. 80°C, 1.0 M methanol, oxygen pressure (gauge) +0:0 bar, +1:1 bar, +2:2 bar. (+0, +1 and +2 in Fig.).

DMFC [17]. When these two factors of temperature and membrane material are allowed for, the recently reported performances of the DMFC are very comparable. For example 0.35 W cm^{-2} at 97°C [5] and 0.385 W cm^{-2} at 130°C [17], both using oxygen at 5 bar.

The use of oxygen in the DMFC clearly has benefits over air in terms of improved power performance. However, most applications of the DMFC will require the use of air as oxidant at a modest pressure. This factor, as well as issues related to safety (in scaling up to an eventual 0.5 kW stack), has meant that scale-up studies have been entirely restricted to the use of air. Fig. 11 shows a performance of the DMFC operating at a temperature of 113°C with 1.0 M methanol solution. The maximum power density is 184 mW cm^{-2}. The performance of the single large-scale cell is generally comparable to that of the small-scale cell in terms of power output and I/V response. However, the performance is not identical.

Typically, we see a somewhat poorer performance with the large-scale cell under what are essentially identical methanol feed conditions. Factors that can explain this include the reproducibility of preparation of MEA for the larger scale. Other major differences in behaviour on scale-up are changes in the fluid temperatures in the cell, the % conversion of methanol achieved and factors affecting the current distribution over the electrode surface. Investigation of these factors is the subject of ongoing research into the scale-up of the DMFC.

An increase in scale of operation of the DMFC will result in changes in the electrical, fluid mechanic and thermal response of the system. The operation of a cell stack contain-

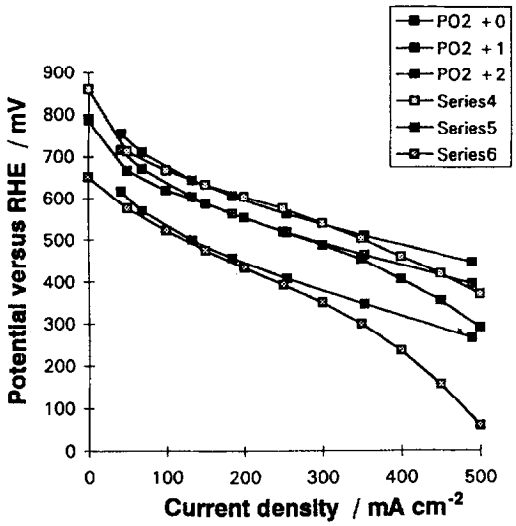

Fig. 10. The effect of methanol crossover on the DMFC performance. 80°C, 1.0 M methanol, oxygen pressure (gauge) +0:0 bar, +1:1 bar, +2:2 bar (+0, +1 and +2 in Fig.). Experimental 4:0 bar, 5:1 bar, 6:2 bar (series 4, 5 and 6 in Fig.).

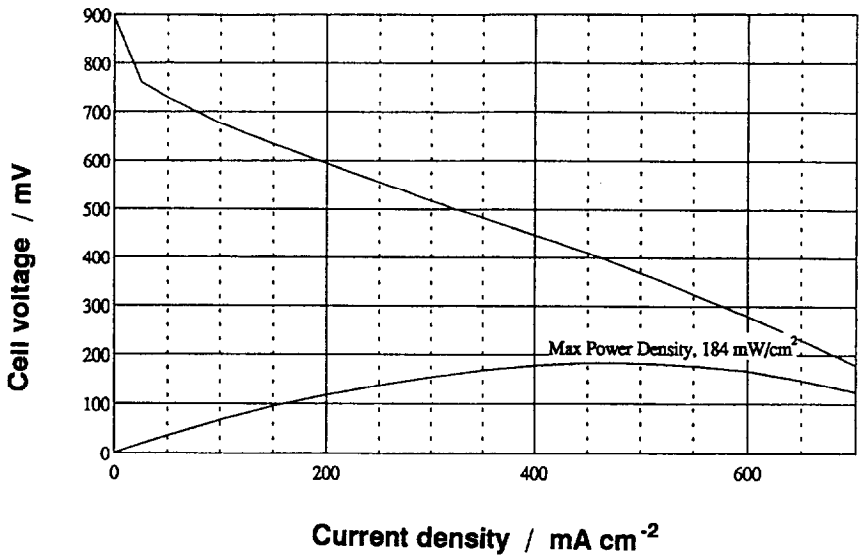

Fig. 11. Performance of the large scale DMFC. 113°C, 1.0 M methanol.

ing, for example, 25–50 membrane/electrode assemblies capable of power output in the range 1–5 kW will require an efficient flow and thermal control system.

Heat generated by the cell stack could be of the same order of magnitude as the designed electrical power output and will be available principally in the exhaust fuel stream and also in the exhaust air. The system will have to perform the following functions:

- supply humidified, pressurised, preheated, clean air
- recover water vapour and methanol (due to crossover) from the exhaust air stream
- supply methanol as a hot aqueous liquid or a vaporised feed
- separate carbon dioxide product gas from the exhaust feed
- recover the heat in the exhaust feed to preheat feed and air streams
- supply methanol to the cell feed to maintain the desired optimum concentration for cell power performance

To study and understand the interactions of the above functions in the fuel cell system, a thermal model of the system itself is used to predict the temperature changes which occur in both fuel and oxidant streams in the cell as a function of cell operating conditions in dynamic operation [18]. A second function of the model is to establish the level of internal temperature changes in the cell which have implications in the mechanical function of MEA components. The components of this model consider that:

(i) Catalyst layers are thin, compared to the membrane, and act as either uniform heat source or sink.

(ii) The bipolar plates have an overall heat transfer coefficient which acts between the two separated fluids.

(iii) The membrane has a high thermal resistance and Joule heat is liberated into both fluids.

(iv) Heat is transferred by flow (electro-osmotic) of water and methanol across the membrane from anode to cathode.

(v) Heat transfer through the porous carbon layers is taken into account.

This model of the MEA will give the required heat flux terms to use in dynamic thermal models of the fluid flow in the channels of the flow beds incorporated into the bipolar plates. The current flow beds used in the DMFC are made as sets of small rectangular channels (approx. 1 mm by 1 mm) arranged in a serpentine flow path. This therefore means that there are seven possible variations in the overall corresponding flows of both fluids; co-, counter- and cross-flow. The above thermal model is solved with a set of equations describing the change in pressures and material balances for methanol consumption, oxygen consumption, water production, and membrane transport and overall mass balances.

5. Conclusions

The results of this work have shown that acceptable performance of the polymer electrolyte DMFC can be achieved at the modest temperature of 80°C using vaporised aqueous methanol feeds. The importance of utilising a high cathode oxygen or air pressure to achieve good performance is also shown. The cell potential versus current density characteristics can be reasonably well predicted using a mathematical model of the MEA based on the variation of reactant concentrations and overpotentials in the catalyst layers. The model also incorporates the influence of methanol crossover from anode to cathode based on a combination of diffusion, electro-osmotic drag, and pressure. At fixed current densities, higher temperatures of operation increase the cell potential and power density values. On scale-up, the cell performance, at the moment, tends to be slightly inferior and this is being explored further. In conjunction with this, research is now under consideration to reduce the extent of methanol crossover and improve the performance of the anode catalysts.

Appendix A. Values of parameters used in the model

ϵ	0.3
b_{cat}	RT/F V/factor of e
b_{an}	$46(T/353)$ mV/factor of e
l_{an}	1.5×10^{-3} cm
l_{ca}	5×10^{-3} cm
n_{an}	6
n_{cat}	4
F	96 488 C/equiv.
$(\gamma i_0)_{cat}$	7.14 A/cm^3 @ 298 K
$E_{0,cat}$	0.355 V
$(\gamma i_0)_{an}$	6.25 A/cm^3 @ 333 K
$E_{0,an}$	0.265 V
P_{an}	1 atm
P_{cat}	2 atm
$\nu_{m,an}$	0.17
$\nu_{m,cat}$	0.05
λ_{H_2O}	2.5 H_2O/H^+
K	$6186\exp(-7100/T)$ cm^2 s^{-1} atm^{-1}
k	$5.926\times10^8\exp(-9756/T)$ cm s^{-1}
t_m	0.0206 cm
$c_{0,MeOH}$	1×10^{-3} mol cm^{-3}
χ	1.51 V/(mol cm^{-2} s^{-1})
T	353 K
R	8.314 J mol^{-1} K^{-1}
λ_{MeOH}	2.48×10^{-2} MeOH/H$^+$
x_{MeOH}	0.0184

Appendix B. Model of the diffusion gas layer

The model for the diffusion mass transfer is described here on the basis that all components are gaseous and well mixed. The purpose of the model is to determine the variation in concentration of species in the porous carbon backing layers and thus the concentration of the reactive species at the edge of the porous catalyst layers. Diffusion in the porous backing layer of the anode can be described using the Stefan–Maxwell equations for a multicomponent gas mixture

$$\nabla x_i=\sum_{j=1}^{n}\frac{RT}{PD_{ij}^{eff}}(x_iN_j-x_jN_i)\quad i=1,2,K,n \tag{A1}$$

N is the molar flux of the appropriate subscript species, x is the mole fraction of the species, and D_{eff} is the effective diffusion coefficient of the i–j species pair. Using the subscripts 1, 2 and 3 for methanol, water and carbon dioxide, respectively, and defining

$$k_{ab}=\frac{RT}{PD_{ab}^{eff}} \tag{A2}$$

we can write

$$\frac{dx_1}{dz}=k_{12}(x_1N_2-x_2N_1)+k_{13}(x_1N_3-x_3N_1) \tag{A3}$$

$$\frac{dx_2}{dz}=k_{21}(x_2N_1-x_1N_2)+k_{23}(x_2N_3-x_3N_2) \tag{A4}$$

$$\frac{dx_3}{dz}=k_{31}(x_3N_1-x_1N_3)+k_{32}(x_3N_2-x_2N_3) \tag{A5}$$

Noting that $k_{ab}=k_{ba}$, and that

$$x_1+x_2+x_3=1 \tag{A6}$$

and noting the stoichiometric equation for the methanol oxidation reaction

$$CH_3OH+H_2O\rightarrow CO_2+6H^++6e^- \tag{A7}$$

so that (assuming no net water transport across the membrane)

$$N_1=N_2=-N_3=N \tag{A8}$$

we can rewrite (A3), (A4), (A5) as

$$\frac{1}{N}\frac{dx_1}{dz}=k_{12}x_1+(k_{13}-k_{12})x_2-k_{13} \tag{A9}$$

$$\frac{1}{N}\frac{dx_2}{dz}=(k_{23}-k_{12})x_1+k_{12}x_2-k_{23} \tag{A10}$$

The solution to these equations is obtained as follows writing

$$Nk_{12}=a\ Nk_{13}=b\ Nk_{23}=c$$

we obtain

$$\frac{dx_1}{dz}=ax_1+(b-a)x_2-b \tag{A11}$$

$$\frac{dx_2}{dz}=(c-a)x_1+ax_2-c \tag{A12}$$

This is a system of first order ODEs: we can rearrange as

$$\frac{d^2x_1}{dz^2}-2a\frac{dx_1}{dz}+(ab-bc+ca)x_1-ab=0 \tag{A13}$$

a second order differential, which can be solved to give (when $(a-b)(a-c)$ is positive)

$$x_1=c_1e^{(a+\beta)z}+c_2e^{(a-\beta)z}+\gamma \tag{A14}$$

$$x_2=\frac{1}{(b-a)}(c_1\beta e^{(a+\beta)z}-c_2\beta e^{(a-\beta)z}+a\gamma+b) \tag{A15}$$

$$x_3=\left(1+\frac{b}{(a-b)}\right)-y\left(1-\frac{a}{(a-b)}\right)-c_1e^{(a+\beta)z}\times\left(1-\frac{\beta}{(a-b)}\right)-c_2e^{(a-\beta)z}\left(1+\frac{\beta}{(a-b)}\right) \tag{A16}$$

where

$$\beta=\sqrt{(a-b)(a-c)}$$

$$\gamma=\frac{ab}{(ab-bc+ca)}$$

$$c_1=\frac{1}{2}\left(x_{10}-\gamma-\frac{1}{\beta}((a-b)x_{20}+a\gamma+b)\right)$$

$$c_2=\frac{1}{2}\left(x_{10}-\gamma+\frac{1}{\beta}((a-b)x_{20}+a\gamma+b)\right)$$

As a first-order approximation it is possible to generate linearised versions of the equations which enable order of magnitude estimates of the impact of diffusion on the variation of concentration in the porous backing layers. This pair of equations can be expanded in a Taylor series around $z=0$ by differentiating wrt z and setting

$$x_1(0)=x_{10}$$

$$x_2(0)=x_{20}$$

thus, to the first term in z,

$$x_1(z)\cong x_{10}+Nz(k_{12}x_{10}+(k_{13}-k_{12})x_{20}-k_{13}) \quad \text{(A17)}$$

$$x_2(z)\cong x_{20}+Nz((k_{23}-k_{12})x_{10}+k_{12}x_{20}-k_{23}) \quad \text{(A18)}$$

and, applying Eq. (A6),

$$x_3(z)\cong x_{30}-Nz(k_{23}x_{10}+k_{13}x_{20}-(k_{13}+k_{23})) \quad \text{(A19)}$$

This approximation is valid for small products, $Nz(k_{ab})$. As a further approximation, in the special case where $k_{12}=k_{13}=k_{23}=k$ we can write

$$x_1(z)\cong x_{10}+Nzk(x_{10}-1)$$

$$x_2(z)\cong x_{20}+Nzk(x_{20}-1)$$

The value of $Nz(k_{ab})$

To evaluate the product $Nz(k_{ab})$ we can write

$$N=\frac{I}{6F},\quad k_{ab}=\frac{RT}{PD_{ab}},\quad l_d\cong 0.25\text{ mm}$$

The PD_{ab} product can be estimated using the Slattery and Bird correlation [19]

$$PD_{ab}=0.0002745\left(\frac{T}{\sqrt{T_a^cT_b^c}}\right)^{1.832}(P_a^cP_b^c)^{1/3}(T_a^cT_b^c)^{5/12}\times\left(\frac{1}{M_a}+\frac{1}{M_b}\right)^{1/2}\epsilon$$

where ϵ represents a correction factor accounting for the porosity and tortuosity of the porous medium: ϵ is commonly found to be between 0.25 and 0.35.

In the case of binary systems containing water, the expression is

$$PD_{ab}=0.0005148\left(\frac{T}{\sqrt{T_a^cT_b^c}}\right)^{2.334}(p_a^cp_b^c)^{1/3}(T_a^cT_b^c)^{5/12}\times\left(\frac{1}{M_a}+\frac{1}{M_b}\right)^{1/2}\epsilon$$

Table A1

	Values of g_{ab} for binary systems in a DMFC		
	H_2O	O_2	CH_3OH
O_2	4.243×10^{-7}		
CH_3OH	1.991×10^{-7}	2.759×10^{-6}	
CO_2	2.731×10^{-7}		2.059×10^{-6}
N_2	4.439×10^{-7}	4.367×10^{-6}	2.768×10^{-6}

Using the Slattery–Bird formulae to calculate values of PD_{ab}, we have

$$PD_{ab}=g_{ab}\epsilon T^{2.334}$$

for systems containing water, and

$$PD_{ab}=g_{ab}\epsilon T^{1.832}$$

otherwise. Values for g_{ab} are given in Table A1.

Using a typical value for ϵ of 0.3, and a temperature of 80°C, the lowest PD_{ab} value is 0.05281 for water/methanol. With a diffusing region 0.3 mm thick, the Nkl product for this system is

$$\frac{RTIl_d}{6FPD}=2.88\times10^{-3}I$$

where I is the current density in A cm^{-2}. This implies that for current densities less than 3 A cm^{-2}, the partial pressures at the catalyst layer will equal the partial pressures in the flow channels with an error of less than 1%.

A similar argument applies to the cathode diffusion region.

Notation

j	permeation rate
$D_{m,i}$	effective diffusion coefficient of i in the membrane
c	concentration
c_1	concentration at feed/membrane interface
c_2	concentration at permeate/membrane interface
Δc	c_2-c_1
F	Faraday constant
t_m	membrane thickness
P	pressure
k	rate of permeate removal
K	constant related to effective hydraulic permeability

x_i	mole fraction of species i
R	gas constant, 8.3143 J/(mol)(K)
P	pressure, atm
D_{ij}^{eff}	effective binary diffusion coefficient for species i, j, cm^2/s
N_i	superficial gas flux of species i, $mol/(cm^2)(s)$
z	direction normal to surface of electrode
x_{io}	mole fraction of species i in the gas flow channel
F	Faraday's constant, 96,488 C/eq
T	temperature
l_d	thickness of gas diffusion layer, cm
superscript c	critical value
I	current density, A cm^{-2}

References

[1] G.L. Troughton, *Ph.D. Thesis*, University of Newcastle, 1992.

[2] J.M. Leger and C. Lamy, *Ber. Bunsenges. Phys. Chem., 94* (9) (1990) 1021–1025.

[3] D.S. Cameron, G.A. Hards, B. Harrison and R.J. Potter, *Platinum Met. Rev., 31* (4) (1987) 173–181.

[4] G.L. Troughton and A. Hamnett, *Bull. Electrochem., 7* (1991) 488.

[5] M.P. Hogarth, *Ph.D. Thesis*, Newcastle University, 1996.

[6] K. Scott, J. Cruickshank and P.C. Christensen, *J. Power Sources*, submitted for publication.

[7] R. Savinell, J.S. Wainwright and S. Wasmus, Nafion/H_3PO_4 as a fuel cell electrolyte for elevated temperature operation, *ISE Conf., Oporto, 1994*, p. V-70.

[8] Executive Summary, *Direct Methanol Fuel Cell Review Meet.*, Dept. of Energy and Advanced Research Projects Agency, Baltimore, 26-27 Apr. 1994.

[9] *NL3BAND.C nonlinear tridiagonal band solver*, © 1991 Technical Software Distributors.

[10] R.E. White, *Ind. Eng. Chem. Fundam., 17* (1978) 367.

[11] T.V. Nguyen and R.E. White, *J. Electrochem. Soc., 140* (1993) 2178.

[12] S.C. Yeo and A. Eisenberg, *J. Appl. Polym. Sci., 21* (1977) 875.

[13] T.E. Springer, T.A. Zawodzinski and S. Gottesfeld, *J. Electrochem. Soc., 138* (1991) 2334.

[14] T.A. Zawodzinski and T.E. Springer, in R.E. White, M.W. Verbrugge and J.F. Stockel (eds.), *Modeling of Batteries and Fuel Cells, Proc. Vol. 91-10*, The Electrochemical Society, Pennington, NJ, 1991, p. 187.

[15] P.S. Kauranen and E. Skou, *J. Appl. Electrochem., 26* (9) (1996) 909.

[16] A. Parthasarathy, S. Srinivasan, A.J. Appleby and C.R. Martin, *J. Electrochem. Soc., 139* (1992) 2530.

[17] X. Ren, M.S. Wilson and S. Gottesfeld, *J. Electrochem. Soc., 143* (1) (1996) L12.

[18] K. Scott, W. Taama and J. Cruickshank, *I. Chem. E. Research Event, Nottingham, 1997.*

[19] J.C. Slattery and R.B. Bird, *J. AIChE, 4* (1958) 137.